A Numerical Investigation on the Electrochemical Behavior of CaO and Al$_2$O$_3$ in the ESR Slags

E. KARIMI-SIBAKI, A. KHARICHA, M. WU, A. LUDWIG, and J. BOHACEK

Field structures including electromagnetic, concentration of ions, and flow fields in an ESR-like process composed of a graphite crucible containing a molten slag, air, and an iron electrode are computed. Both CaF$_2$—(mass pct 2) CaO and CaF$_2$—(mass pct 2) Al$_2$O$_3$ slags are examined. Tertiary current distribution is calculated. Therefore, polarization overpotential and Faradic reactions at metal–slag interface are considered using Tafel law, whereas transport of ions in the bulk of slag is determined through Nernst–Planck equations. The main goal is to shed light on the invisible phenomena such as magnetohydrodynamics caused by transport of ions, electrical conductivity of CaF$_2$-based slag using additives (*e.g.*, CaO or Al$_2$O$_3$), and the role of complexation of ions (*e.g.*, AlO$_3^{3-}$) in the molten slag applied to the ESR. An explanation is given for the observation of higher oxygen content in the metal using Al$_2$O$_3$ than that using equivalent amount of CaO in the CaF$_2$-based slag of a DC-operated ESR.

I. INTRODUCTION

MASS transfer is a major phenomenon occurring in electroslag remelting (ESR) process.[1,2] Different contributions of mass transfer are easily recognized in removal and precipitation of non-metallic inclusions in the slag and melt pool,[3,4] refinement of the alloy,[5–7] and chemical and electrochemical reactions in the slag through the process.[8,9] Numerous electrochemical (faradaic) reactions take place at the slag–metal interface aiming at obtaining an alloy ingot which is clean and chemically refined. For instance, faradaic reactions of alloying elements such as Ti, S, O, Fe, Ca, and Al were reported.[8] The CaF$_2$-based slag, typically composed of CaF$_2$, CaO, and Al$_2$O$_3$, serves as the electrolyte in ESR. Thereby, the electrochemical transport of ions such as Ca^{2+}, Al^{3+}, Fe^{2+}, F$^-$, and O^{2-} plays a crucial role in the electrical conductivity of the slag and consequently the performance of the process.

Several observed phenomena during DC operation of ESR were attributed to the ionic properties of the molten slag. The melt rate of the ESR electrode with positive polarity as known as direct current reverse polarity (DCRP) was observed *in situ* to be higher than that for the ESR electrode with negative polarity as known as direct current straight polarity DCSP.[10–12] Mitchell *et al.*[13,14] reported the formation of a thick layer of iron oxide (FeO) under the tip of electrode in the DC-operated ESR-like process. Kato *et al.*[15] noticed higher oxygen content in the ingot for the ESR process operated by DCRP than that of DCSP. Additionally, Kojima *et al.*[16] detected higher oxygen content in the ingot using CaF$_2$—(mass pct 20) Al$_2$O$_3$ slag than that using CaF$_2$—(mass pct 20) CaO slag in the ESR operated by DCSP.

Modeling attempts were made to investigate chemical and electrochemical reactions in the slag of ESR by means of thermodynamics and kinetic modeling approach.[17–19] One should consider that the ESR process is inherently an electrochemical system. Therefore, it is of great importance to develop electrochemical model capable of describing the ion transport in the bulk of slag and electrochemical reactions at slag–metal interfaces for an ESR process. For this purpose, we propose a numerical model in the present study.

Transport phenomena in an ESR-like system composed of an electrode made of pure iron, molten slag (electrolyte), air, and graphite crucible (see Figure 1) are calculated. The electromagnetic field is modeled in the entire system. The interplay between the concentration

---

E. KARIMI-SIBAKI and A. KHARICHA are with the Christian-Doppler Laboratory for Metallurgical Applications of Magnetohydrodynamics, Montanuniversitaet of Leoben, Franz-Josef-Str. 18, 8700 Leoben, Austria. M. WU, A. LUDWIG, and J. BOHACEK are with the Chair of Simulation and Modeling of Metallurgical Processes, Montanuniversitaet of Leoben, Franz-Josef-Str. 18, 8700 Leoben, Austria. Contact e-mail: Abdellah.kharicha@unileoben.ac.at
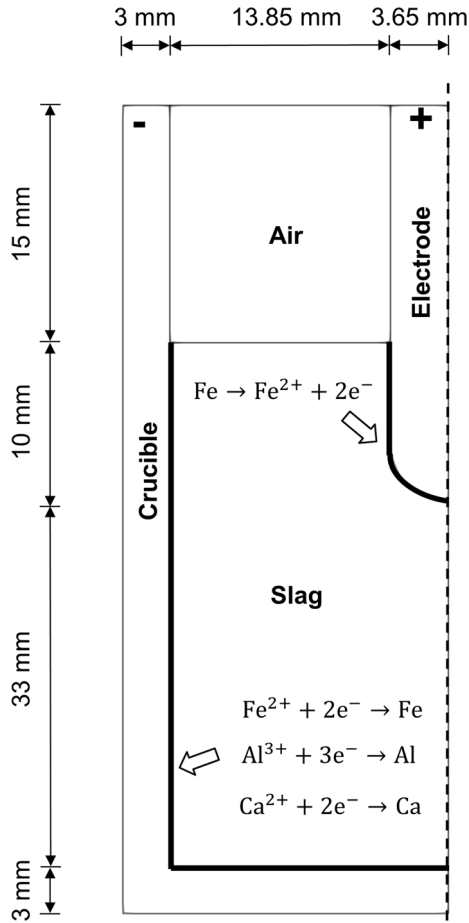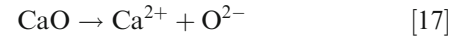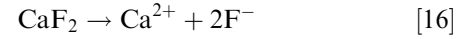
Fig. 1—Configuration of the computational domain and boundaries are illustrated. In all calculations, electrode is anode (+) and graphite crucible is cathode (−).

of ions, electromagnetic, and flow fields in the slag is taken into account according to tertiary current distribution approach.[20,21] Correspondingly, Faradic reactions at metal–slag interface are described using Tafel law,[22] whereas transport of ions in the bulk of slag is determined through Nernst–Planck equations.[21] Two different slags are examined: CaF_2—(mass pct 2) CaO and CaF_2—(mass pct 2) Al_2O_3. The ultimate goal is to obtain some fundamental understanding of the contribution of electrochemical transport/reaction of ions in the slag to the outcome of a DC-operated ESR. Based on the modeling results, we put forward an explanation for a phenomenon, namely, higher oxygen content in the ingot using CaF_2-Al_2O_3 slag than that using CaF_2-CaO slag in the ESR operated under DCSP.[16]

II. MODELING

All symbols used in this paper are listed in Nomenclature. Governing equations including Eqs. [1] to [15] are listed in Table I, and they will be further elucidated in this section. For the sake of simplicity and to avoid extra complexity, the following assumptions are made:

(i) The electrolytes (molten slags) are assumed to be fully dissociated at the elevated temperature of the process (~ 1803 K). Therefore, all molecules of the slags split to ions as follows:

$$CaF_2 \rightarrow Ca^{2+} + 2F^- \quad [16]$$

$$CaO \rightarrow Ca^{2+} + O^{2-} \quad [17]$$

$$Al_2O_3 \rightarrow 2Al^{3+} + 3O^{2-} \quad [18]$$

$$Al_2O_3 \rightarrow Al^{3+} + AlO_3^{3-} \quad [19]$$

(ii) Formation of oxyfluorides (e.g., AlF_6^{3-}, $AlOF_2^-$, $AlO_2F_2^{3-}$) and any other chemical reactions like generation/recombination that may occur in the molten CaF_2-based slag is not included in the model.[23–25] As described in Eq. [19], only complexation of the well-known aluminate ion (AlO_3^{3-}) is taken into account.[15,16]

(iii) The faradaic reaction of the oxidation of iron ($Fe \rightarrow Fe^{2+} + 2e^-$) is considered at the anode, whereas the following reactions take place at the cathode:

$$Fe^{2+} + 2e^- \rightarrow Fe \quad [20]$$

$$Ca^{2+} + 2e^- \rightarrow Ca \quad [21]$$

$$Al^{3+} + 3e^- \rightarrow Al \quad [22]$$
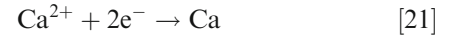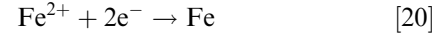
There exists initially no Fe^{2+} in the slag, thus other ions (e.g., Ca^{2+} or Al^{3+}) must react to deliver the electric current to the cathode. As time advances, sufficient amount of Fe^{2+} can reach to the cathode to participate to faradaic reactions through Eq. [20]. Ca^{2+}, Al^{3+}, and Fe^{2+} compete to gain electron as described in Eqs. [20] through [22] at the cathode. The priority to gain the electron is dependent on the standard reduction potential [26] as follows: first (Fe^{2+}), second (Al^{3+}), and third (Ca^{2+}). The neutral Al, Fe, and Ca atoms are ignored in the calculations.

(iv) The formation of electric double layer (EDL) exerts a potential drop (jump) at the anodic electrode–electrolyte (slag) interface.[26,27] That is implicitly modeled through Tafel equation: $j = j_0 e^{-\frac{\eta}{b}}$. The active area of the cathodic crucible is much larger (by a factor of twenty) than that of the anodic electrode, and consequently, the amount of electric current density that flows through the cathode is minimal. As such, the electric potential jump due to the formation of EDL is assumed to be negligible at crucible–slag interface. As the electro-active Fe^{2+} has the highest priority to gain the electron, the value of the concentration of Fe^{2+} is set to zero at the cathode.

Table I. Governing Equations of Flow, Magnetic, Concentration of Ions, and Electric Current Density Fields

Flow field

$$\frac{\partial \rho}{\partial t} + \nabla \cdot (\rho \vec{u}) = 0 \tag{1}$$

$$\frac{\partial(\rho \vec{u})}{\partial t} + \nabla \cdot (\rho \vec{u} \vec{u}) = -\nabla p + \nabla \cdot \left[\mu (\nabla \vec{u} + \vec{u}^{\mathrm{T}}) \right] + \rho \vec{g} + \vec{F}_{\mathrm{L}} \tag{2}$$

$$\vec{F}_{\mathrm{L}} = \vec{j} \times \vec{B} \tag{3}$$

Magnetic field

$$\vec{B} = \nabla \times \vec{A} \tag{4}$$

$$\nabla \times \left[\frac{1}{\mu_0} \nabla \times \vec{A} \right] = \vec{j} \tag{5}$$

Electric current density and ion concentration fields

$$\nabla \cdot \vec{j} = 0 \tag{6}$$

$$\vec{j} = -\sigma \nabla \varphi \text{ (In metal)} \tag{7}$$

$$\vec{j} = F \sum_i z_i \vec{N}_i \text{ (In slag)} \tag{8}$$

$$\vec{N}_i = \vec{u} c_i - D_i \nabla c_i - \frac{z_i D_i F \nabla \varphi}{RT} c_i \tag{9}$$

$$i = Ca^{2+}, Fe^{2+}, Al^{3+}, F^-, O^{2-}, AlO_3^{3-}$$

$$\frac{\partial c_{Ca^{2+}}}{\partial t} = -\nabla \cdot \vec{N}_{Ca^{2+}} \tag{10}$$

$$\frac{\partial c_{Fe^{2+}}}{\partial t} = -\nabla \cdot \vec{N}_{Fe^{2+}} \tag{11}$$

$$\frac{\partial c_{Al^{3+}}}{\partial t} = -\nabla \cdot \vec{N}_{Al^{3+}} \tag{12}$$

$$\frac{\partial c_{O^{2-}}}{\partial t} = -\nabla \cdot \vec{N}_{O^{2-}} \tag{13}$$

$$\frac{\partial c_{AlO_3^{3-}}}{\partial t} = -\nabla \cdot \vec{N}_{AlO_3^{3-}} \tag{14}$$

$$z_{F^-} c_{F^-} = -\left[z_{Ca^{2+}} c_{Ca^{2+}} + z_{Fe^{2+}} c_{Fe^{2+}} + z_{Al^{3+}} c_{Al^{3+}} + z_{O^{2-}} c_{O^{2-}} + z_{AlO_3^{3-}} c_{AlO_3^{3-}} \right] \tag{15}$$

(v) We assumed that the electric current is carried only by the movement of ions so that any possible electronic conduction within the molten slag is ignored.[28]

(vi) The bulk of slag always remains electrically neutral.[26] Mathematically, the bulk electro-neutrality is expressed as follows: $\sum_i z_i c_i = 0, i = Ca^{2+}, Fe^{2+}, Al^{3+}, F^-, O^{2-}, AlO_3^{3-}$.

(vii) To the best of our knowledge, diffusion coefficients of involving ions are unknown, as they are dependent on several parameters such as temperature, pressure, electrolyte composition, radius, and valency of diffusing ions.[23] Herein, an identical value $(5 \times 10^{-9} \text{ m}^2 \text{ s}^{-1})$ is assumed for all ions.

(viii) The solutal buoyancy force as a consequence of the spatial variation in the ion concentration fields is ignored. The isothermal flow in the molten slag is exclusively driven by Lorentz force.

The induced magnetic field is dominantly azimuthal so that a 2D axisymmetric computational domain is considered as illustrated in Figure 1.

A. *Governing Equations*

All governing equations to calculate flow, magnetic, electric current density, and ion concentration fields are listed in Table I.

As described in Eqs. [1] and [2], the flow field in the slag zone is determined by solving continuity and momentum equations. The source term in momentum equation is the Lorentz force that is calculated using Eq. [3]. The slag–air interface is assumed to remain stationary where a condition of free-slip is assigned. No-slip boundary condition is applied at all other boundaries. The flow is not calculated in the air zone.

As described in Eqs. [4] to [5], the A–φ formulation is used to calculate the magnetic field in the entire system.[29,30] The Coulomb gauge ($\nabla \cdot \vec{A} = 0$) is utilized to achieve a unique solution for magnetic vector potential.[29] A constant value for the magnetic permeability is assumed in the entire domain. Radial and axial components of magnetic vector potential are set zero at crucible side and crucible bottom. The flux of magnetic

vector potential is set zero at the top of electrode, top of air, and top of crucible.[21] Continuity of the magnetic field is applied at all interior boundaries.

The conservation equation of electric current density, Eq. [6], is solved in the entire domain. Ohm's law, Eq. [7], is applied for crucible and electrode, whereas Nernst–Planck equations including Eqs. [8] to [15] are used to calculate electric current density in the slag. The total mass flux of each ion, Eq. [9], is composed of advection flux, diffusion flux, and electro-migration flux. As described through Eqs. [10] to [14], the total flux of each ion must be conserved. The imposition of electro-neutrality, assumption (vi), provides a simplification. The concentration field of one non-reacting ion (here F^-) is evaluated using the ion concentration fields of other involving ions as described in Eq. [15].

Boundary conditions for electric potential and concentrations of ions are interdependent.[21] The total mass flux (advection + diffusion + migration) of non-reacting ions is zero at all boundaries. A positive mass flux related to the electric current density is assigned for Fe^{2+} at the anodic electrode–slag interface: $j = z_{Fe^{2+}} F \vec{N}_{Fe^{2+}}$.

As previously mentioned in assumption (iii), Fe^{2+} has higher standard reduction potential compared to that of Ca^{2+} and Al^{3+}.[26] Therefore, the electro-active Fe^{2+} has the highest priority to gain the electron so that the value of the concentration of Fe^{2+} is set to zero at the cathodic crucible–slag interface. As all reacting ions (Fe^{2+}, Ca^{2+}, and Al^{3+}) contribute to deliver the electric current from the slag to the cathode, the mass fluxes of Ca^{2+} and Al^{3+} can be determined through $j = z_{Fe^{2+}} F \vec{N}_{Fe^{2+}} + z_{Ca^{2+}} F \vec{N}_{Ca^{2+}} + z_{Al^{3+}} F \vec{N}_{Al^{3+}}$.

At the top of mold, the electric potential is set zero. The flux of electric potential ($\approx$ electric current density) is assigned (5 A cm^{-2}) at the top of electrode to ensure equal amount of electric current density flows through the system regardless of the electric conductivity of slags which are CaF$_2$—(mass pct 2) CaO or CaF$_2$—(mass pct 2) Al$_2$O$_3$. The continuity of electric field is considered in all interior boundaries. However, special care must be taken to define boundary condition for electric potential at anodic electrode–slag interface where the fluxes of electric potential ($\approx$ electric current density) on both sides of the conjugate wall are equal to each other, whereas electric potential magnitudes are unequal as a consequence of the formation of EDL. The discontinuity (jump) in the electric potential is assigned through Tafel law as described in assumption (iv). The relationship between electric current density and overpotential (potential jump) for the aforementioned slags is plotted in Figure 2. A simple regression analysis helps us to obtain the parameters required in Tafel law.[21] The experimental measurements are reproduced from Reference 13.

B. *Other Settings*

Mitchell *et al.*[13] performed a series of experiments in an ESR-like apparatus using the galvanostatic pulsing technique to measure the polarization overpotential at the interface between the metal and CaF$_2$-based electrolytes. The electrode made of pure iron was immersed into an isothermal ($\sim$ 1803 $\pm$ 5 K) CaF$_2$-based slag. A molybdenum-lined graphite crucible was used. Herein, the model is configured based on their study. Mitchell *et al.*[13] pointed out that the condition of this experiment represents an actual DCSP ESR ingot. The 2D axisymmetric configuration of the system is presented in Figure 1, and details of the experiment are described in Reference 13.

A very fine mesh involving 0.2 million volume elements was generated. The smallest computational mesh element is ca. 30 μm near the electrode. The size of mesh elements smoothly and incrementally increases away from the electrode toward the bulk of electrolyte using a successive ratio of 5 pct. The commercial software FLUENT-ANSYS v. 14.5 was used to implement modeling equations by the help of user-defined functions (UDF). The software employs finite volume method (FVM).[31] FVM is extensively used to precisely model the flow field. Additionally, mass conservations of all ions are automatically satisfied. The first-order implicit method is used for temporal discretization of governing equations.[31] The spatial discretization is based on the third-order MUSCL scheme in which variable grid sizes and strong advection/migration flux are accurately handled.[32] The pseudo-transient computation technique was utilized to perform transient calculations aiming at achieving steady-state solution.[33] Correspondingly, the transient terms (temporal derivatives) for all governing equations were retained,[31] as described in Table I. This technique is effective to obtain the steady-state solution of complex problems involving non-linear equations when the initial iterate is far from the final solution. The steady-state results were subject to further evaluation. All parameters used in our calculations are listed in Table II.

III. RESULTS

A series of simulations was performed to investigate the effect of slag type, *e.g.*, CaF$_2$—(mass pct 2) CaO and CaF$_2$—(mass pct 2) Al$_2$O$_3$ on magnetohydrodynamics (MHD) and electrochemical behaviors of the system.
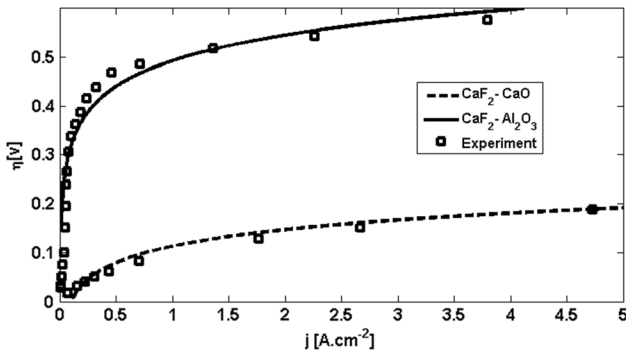

Fig. 2—The total overpotential is plotted against the amount of imposed electric current considering following slags: CaF$_2$—(mass pct 2) CaO and CaF$_2$—(mass pct 2) Al$_2$O$_3$.

Table II. Parameters Used in Our Calculations

Parameter	Unit	
μ_0	H m^{-1}	$4\pi \times 10^{-7}$
R	J K^{-1}mol^{-1}	8.314546
g	m s^{-2}	9.81
T	K	1803
F	A s mol^{-1}	96,485
I	A	1
$\sigma_{\text{Electrode}}$	S m^{-1}	8×10^5
σ_{Crucible}	S m^{-1}	2×10^5
σ_{Air}	S m^{-1}	10^{-10}
σ_{Slag}	S m^{-1}	Calculated
ρ	kg m^{-3}	2550
μ	kg s^{-1}m^{-1}	0.005
j_0	A m^{-2}	1000 and 20
b	V	0.049 and 0.076
$z_{\text{Ca}^{2+}}$	—	+ 2
$z_{\text{Fe}^{2+}}$	—	+ 2
$z_{\text{Al}^{3+}}$	—	+ 3
$z_{\text{F}^{-1}}$	—	− 1
$z_{\text{O}^{2-}}$	—	− 2
$z_{\text{AlO}_3^{3-}}$	—	− 3
$D_i\left(i = \text{Ca}^{2+}, \text{Fe}^{2+},\right.$ $\left.\text{Al}^{3+}, \text{F}^-, \text{O}^{2-}, \text{AlO}_3^{3-}\right)$	m^{2}s^{-1}	5×10^{-9}

Demonstratively, field structures for the system involving CaF$_2$—(mass pct 2) CaO are shown in Figure 3. The magnetic field is strong in the vicinity of the lateral wall of the electrode where the highest amount of electric current density flows through the slag. The intensity diminishes gradually away from the electrode toward the bulk of slag as shown in Figure 3(a). The flow is exclusively driven by Lorentz force that in turn is originated in the electromagnetic field. As shown in Figure 3(b), the highest magnitude of Lorentz force and consequently the highest magnitude of velocity are observed near the electrode where both magnetic field and electric current density are strong. The electric current spreads radially outwards near the electrode–slag interface that results in the formation of a rotational Lorentz force field. Consequently, a vortical flow develops which is known as electro-vortex flow. The concentration fields of involving ions are shown in Figure 3(c) through (d). Expectedly, cations (e.g., Ca^{2+}) accumulate near the crucible cathode, whereas anions (e.g., F$^-$ and O^{2-}) move toward the anodic electrode. The electro-migration assists the transport of cations (e.g., Fe^{2+}, Ca^{2+}) by advection toward the cathodic crucible. In contrast, electro-migration competes against advection to transport anions (e.g., F$^-$ and O^{2-}) toward the anodic electrode. As shown in Figure 3(d), the concentration of Fe^{2+} is notably highly adjacent to the electrode–slag interface where Fe^{2+} is injected into the slag. Contrastingly, the concentration of Fe^{2+} is very low near the crucible where Fe^{2+} is removed from the slag by a faradaic reaction (Eq. 20). Ca^{2+} as a cation accumulates near the cathode as shown in Figure 3(c). In the absence of Fe^{2+}, the electric current is delivered from the slag to the crucible by faradaic reaction of Ca^{2+} (Eq. 21). Thus, a non-uniform concentration of

Ca^{2+} is observed in the vicinity of crucible as higher amount of electric current flows to the crucible near the free surface of slag.

As previously mentioned, the slag containing Al$_2$O$_3$ may form complexes of polyatomic ions such as AlF$_6^{3-}$, AlO$_2$F$_2^{3-}$, AlO$_2$F$_2^{3-}$, and AlO$_3^{3-}$. It is difficult to estimate the amount of each of those complexes in the slag. For that purpose, quantum mechanical approach using density functional theory (DFT) is required[34] that is beyond the scope of the present study. It is believed that the aluminate ion (AlO$_3^{3-}$) is the common product of the dissociation of Al$_2$O$_3$ in the slag as described in Eq. [19]. Therefore, two different dissociation reactions are considered through Eqs. [18] and [19] to investigate the electrochemical behavior of CaF$_2$—(mass pct 2) Al$_2$O$_3$ slag. A summary of results is shown in Figure 4. Three situations are examined: firstly, dissociation to form only O^{2-} according to Eq. [18], secondly, dissociation to form only AlO$_3^{3-}$ according to Eq. [19], and thirdly, dissociation to form equivalent amount of O^{2-} and AlO$_3^{3-}$ based on both Eqs. [18] and [19]. Both O^{2-} and AlO$_3^{3-}$ exhibits the highest concentrations near the electrode–slag interface as they migrate toward the anode.

The formation of aluminate complex remarkably reduces the concentration of free O^{2-} that in turn decreases the overall electrical conductivity of the slag as shown in Figure 5. The electrical conductivity of the slag is related to the concentration of involving ions as follows: $\sigma_{Slag} = \sum_i \frac{z_i^2 D_i F^2}{RT} c_i$.[26] The electrical conductivity is non-uniform within the slag. The highest electrical conductivity is near the electrode where an enormous amount of Fe^{2+} is injected into the slag. Evidently, the electrical conductivity decreases as the amount of complex ions increases. Formation of complex ions can increase the solubility of the slag that enables us to improve the efficiency of refining in the ESR. However, increasing the amount of Al$_2$O$_3$ in the slag leads to further formation of complex ions such as AlF$_6^{3-}$, AlO$_2$F$_2^{3-}$, AlO$_2$F$_2^{3-}$ that in turn further reduces the mobility of F$^-$ and consequently the electrical conductivity. These results are in accordance with observations of Mitchell et al.[24] and Birol et al.[35] on electrical conductivity of CaF$_2$-Al$_2$O$_3$ slag. They pointed out that adding a relatively small amount of Al$_2$O$_3$ can drastically decrease the electrical conductivity of slag as a consequence of formation of polyatomic complexes.

IV. DISCUSSIONS

Mitchell et al.[13] designed the apparatus (shown in Figure 1) with the purpose of formulating electrochemical reaction mechanisms for charge transfer at metal–slag interface under ESR conditions. In the experiment, the cathodic electrode represents DCRP while the anodic electrode is tantamount to DCSP condition in ESR. As such, the behavior of the electrode in this study imitates an actual ESR ingot during DCSP.[13] For the
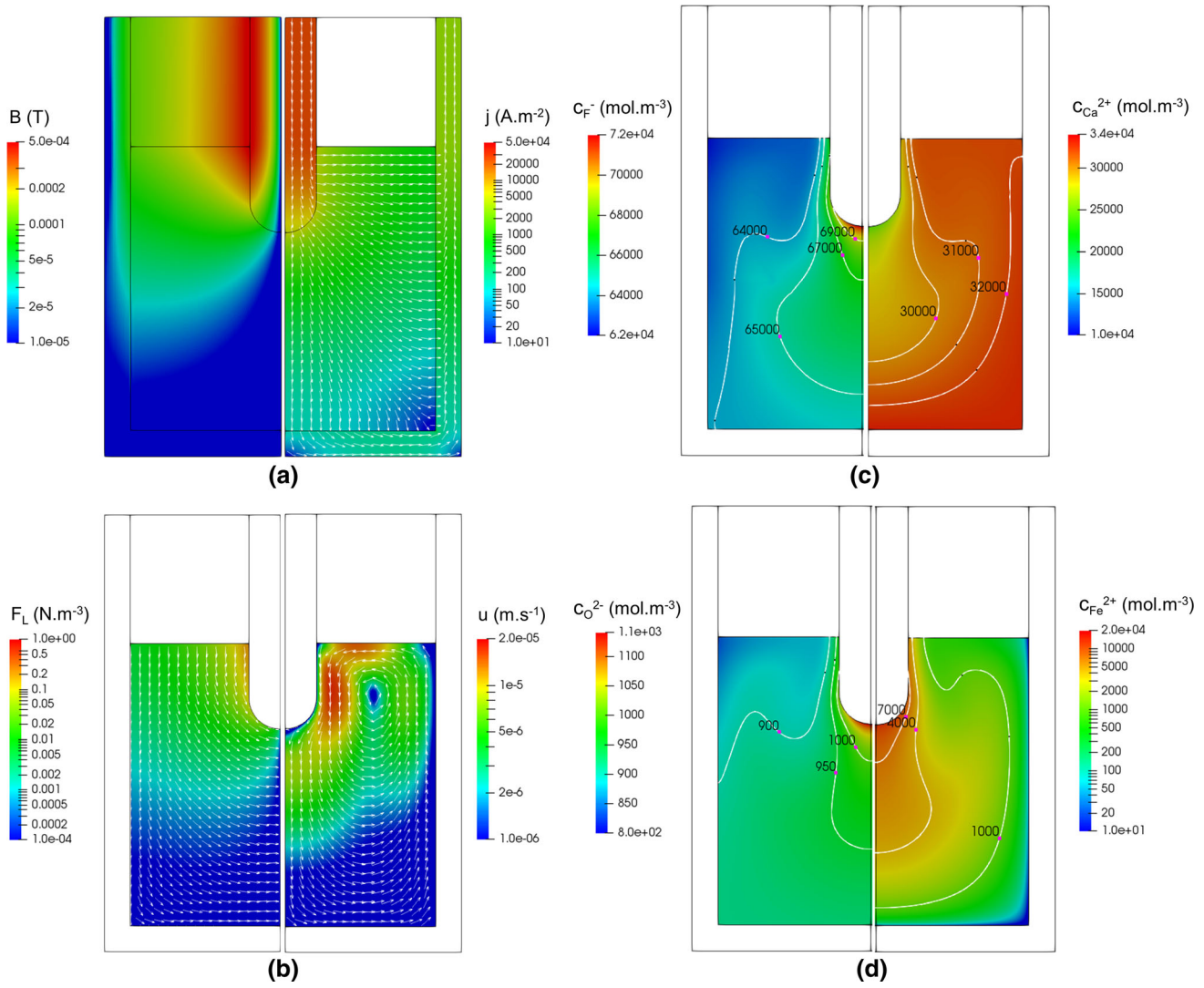
Fig. 3—Field structures are shown for the system involving CaF$_2$—(mass pct 2) CaO slag; (*a*) magnetic field (left half) and electric current density (right half); (*b*) Lorentz force field (left half) and velocity field (right half); (*c*) concentration field of F$^-$ (left half) and concentration field of Ca^{2+} (right half); (*d*) concentration field of O^{2-} (left half) and concentration field of Fe^{2+} (right half);.

latter, a higher oxygen content in the ingot using CaF$_2$—Al$_2$O$_3$ slag than that using CaF$_2$-CaO slag was observed when equivalent amount of Al$_2$O$_3$ and CaO were used.[13–16] The dissociation of CaO is well recognized by Eq. [17]. Although numerous dissociations for Al$_2$O$_3$ are plausible in the molten slag, the simultaneous increase of [Al] and [O] in the ingot by DCSP could be elucidated as follows [15,16]:

$$O^{2-} - 2e^- \rightarrow [O] \qquad [23]$$

$$AlO_3^{3-} - 3e^- \rightarrow \frac{1}{2}[Al_2O_3] + \frac{3}{2}[O] \qquad [24]$$
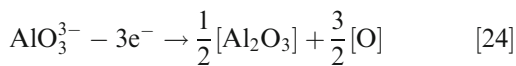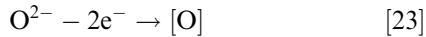
Oxygen is provided to the ingot through the discharge reaction, Eq. [23]. Meanwhile, the discharge of aluminate ion, Eq. [24], dispenses oxygen and Al$_2$O$_3$ that is precipitated as inclusions in the ingot. Figure 6 is

illustrated to identify the contribution of aforementioned reactions including Eqs [17], [23], and [24] on the amount of final Oxygen in the metal. Four situations are examined: firstly, complete dissociation of CaO to form O^{2-} according to Eq. [17], secondly, complete dissociation of Al$_2$O$_3$ to form O^{2-} according to Eq. [18], thirdly, complete dissociation of Al$_2$O$_3$ to form AlO$_3^{3-}$ according to Eq. [19], and fourthly, dissociation of Al$_2$O$_3$ to form equivalent amount of O^{2-} and AlO$_3^{3-}$ based on both Eqs. [18] and [19].

Complete dissociation of Al$_2$O$_3$ to form AlO$_3^{3-}$ according to Eq. [19] results in a lower amount of oxygen in the metal compared to that of using CaO. This conflicts the experimental observation, namely, higher oxygen content in the ingot using CaF$_2$-Al$_2$O$_3$ slag than that using CaF$_2$-CaO slag.[13–16] Therefore, aluminate cannot be the only complex in the slag which was pointed out also by Kojima et al.[16] They estimated
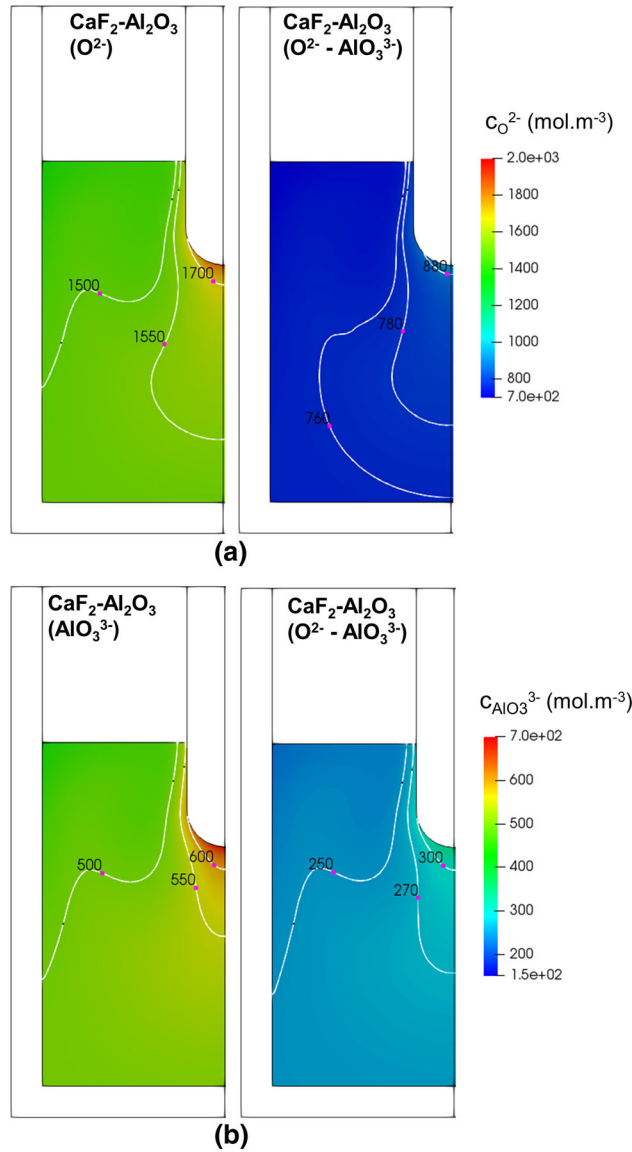
Fig. 4—Concentration fields of O^{2-} and AlO_3^{3-} are shown for the system involving CaF_2—(mass pct 2) Al_2O_3 slag. Each contour is labeled according to the involved ions in the system; (a) concentration field of O^{2-}; (b) concentration field of AlO_3^{3-}. The dissociations are expressed as follows: (O^{2-}) only O^{2-} exists; (AlO_3^{3-}) only complex ion AlO_3^{3-} exists; (O^{2-}-AlO_3^{3-}) the dissociation is assumed to provide 50 pct O^{2-} and 50 pct AlO_3^{3-}.

that 40 pct to 60 pct of the oxygen is carried by aluminate ion to the metal which is considered in simulation results and confirmed by experimental observation.

Of note, the presented model in this study was successfully verified.[11,12,21,27] Herein, we lack experimental data such as velocity or concentrations of ions within the electrolyte, to further validate our model. Generally, experimental measurements are difficult due to the opacity of materials at high temperature (~ 1800 K) of electro-metallurgical processes. Nevertheless, the presented model helps us to shed light on the electrochemical behavior of ESR process considering

electrical conductivity of CaF_2-based slag using additives such as CaO or Al_2O_3, the role of complexation of ions, magnetohydrodynamics (MHD) in the slag, *etc.*

V. SUMMARY

A 2D axisymmetric model is presented to investigate transport phenomena in an ESR-like system comprises a graphite crucible, air, and an electrode made of pure iron which is immersed into a molten slag at elevated temperature (~ 1803 K). The system had been designed aiming at investigating mechanisms for charge transfer at metal–slag interface under real ESR conditions. Herein, the electrode is anodic that in turn represents the condition of direct current straight polarity (DCSP) in a DC-operated ESR process. The electromagnetic field is computed in the entire system. The interplay between flow and electromagnetic field as known as magnetohydrodynamics (MHD) is calculated in the molten slag. The model takes into account the interaction between the concentration fields of ions and electric current density field through Nernst–Planck equations in the bulk of slag. The polarization overpotential including faradaic reactions and concentration overpotential at the anodic electrode–slag is modeled through Tafel law. Two slags are examined, namely, CaF_2—(mass pct 2) CaO and CaF_2—(mass pct 2) Al_2O_3. Accordingly, electrochemical transports of following ions are calculated: Ca^{2+}, Fe^{2+}, Al^{3+}, F^-, O^{2-}, AlO_3^{3-}. A summary of main conclusions is drawn as follows:

- Anions such as (F^-, O^{2-}, AlO_3^{3-}) can reach and consequently accumulate near the anodic electrode–slag interface although the electro-vortex flow competes against the electro-migration of anions. This implies that the electro-migration can surpass the advection of anions. Of note, the solutal buoyancy force is not taken into account in the model which can influence the velocity field and consequently the advection flux of ions. As such, it is necessary to include buoyancy in the future model.

- The electric conductivity in the bulk of slag is non-uniform. Regardless of the slag type, the highest value of electrical conductivity is observed under the electrode where a tremendous amount of Fe^{2+} is injected into the slag. In contrast, the lowest value of electrical conductivity is observed near the crucible where cations are consumed through faradaic reactions.

- Complexation of aluminate ion (AlO_3^{3-}) is taken into account. Although diffusion coefficients of all involving ions are assumed to be identical, the electrical conductivity in the bulk of slag decreases as the amount of aluminate ion increases.

- Aluminate ion is believed to be the utmost complex in the slag. In DCSP-operated ESR, a higher oxygen content in the ingot using CaF_2-Al_2O_3 slag than that using CaF_2-CaO slag was observed when equivalent amount of Al_2O_3 and CaO was used. Simulation results reveal that complete dissociation of Al_2O_3 to form AlO_3^{3-} leads to a lower amount of oxygen in the
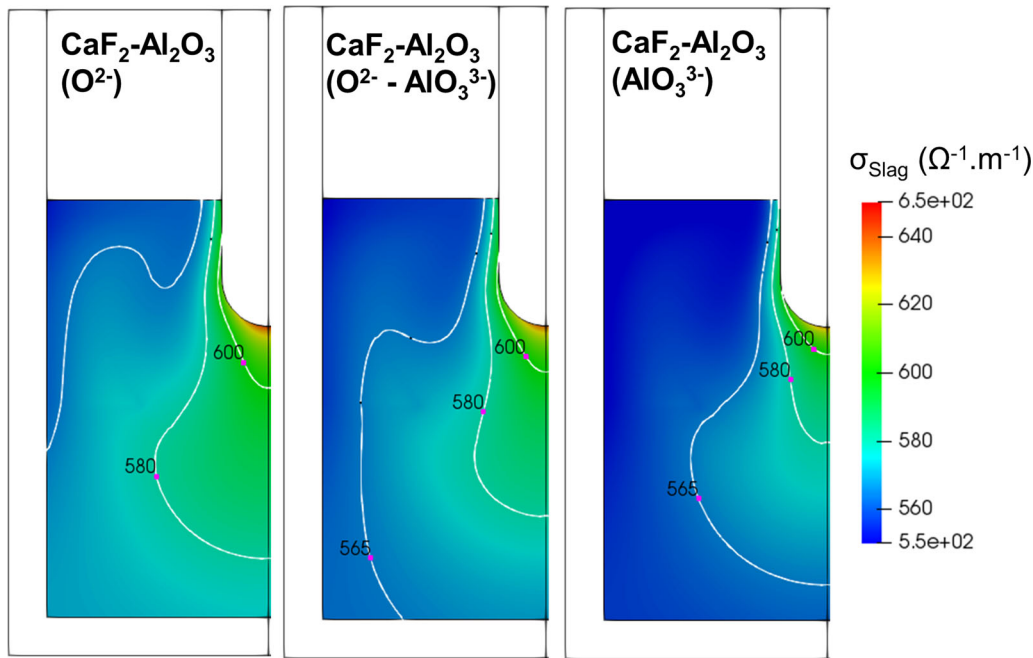
Fig. 5—Distribution of electrical conductivity within the slag is illustrated for the system involving CaF_2—(mass pct 2) Al_2O_3 slag. Each contour is labeled according to the involved ions in the system; (O^{2-}) only O^{2-} exists; (AlO_3^{3-}) only complex ion AlO_3^{3-} exists; (O^{2-}-AlO_3^{3-}) the dissociation is assumed to provide 50 pct O^{2-} and 50 pct AlO_3^{3-}.
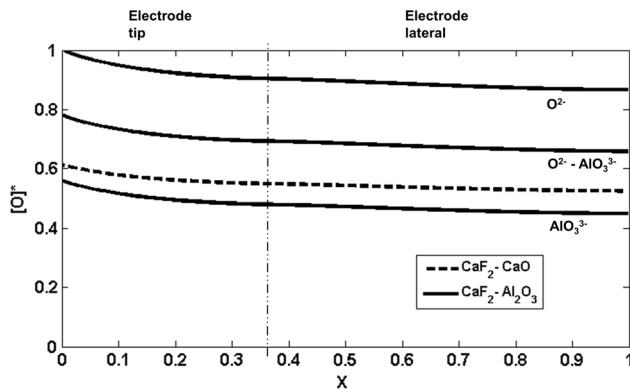

Fig. 6—The normalized amount of precipitated oxygen in the metal is plotted across lateral wall and tip of electrode for both slags. Curves are labeled for the system involving CaF_2—(mass pct 2) Al_2O_3 slag considering existence of only O^{2-}, existence of only AlO_3^{3-}, and existence of 50 pct O^{2-} and 50 pct AlO_3^{3-}.

final ingot compared to that of using CaO. Therefore, complexation of other ions like AlF_6^{3-}, $AlO_2F_2^{3-}$, $AlO_2F_2^{3-}$ must occur.

Despite being a fundamental research, the present study provides insights into the invisible phenomena such as magnetohydrodynamics (MHD) caused by transport of ions, electrical conductivity of CaF_2-based slag using additives (e.g., CaO or Al_2O_3), and the role of complexation of ions in the molten slag applied to the real DC-operated ESR process.

NOMENCLATURE

$\vec{A}$	Magnetic vector potential, V s m^{-1}
$\vec{B}$	Magnetic field, T
b	Tafel slope, V
c	Concentration of each ion, mol m^{-3}
D	Diffusion coefficient of each ion, m^{2}s^{-1}
F	Faraday constant, A s mol^{-1}
$\vec{F}_L$	Volumetric Lorentz force, N m^{-3}
g	Gravity constant, m s^{-2}
I	Imposed electrical current, A
j	Electric current density, A m^{-2}
j_0	Exchange current density in Tafel equation, A m^{-2}
$\vec{N}$	Total flux of each ion, mol m^{-2}s^{-1}
p	Pressure, Pa
R	Universal gas constant, J K^{-1} mol^{-1}
t	Time, s
T	Temperature, K
$\vec{u}$	Velocity vector, m s^{-1}
X	Dimensionless distance
z	Charge number of each ion
ρ	Density, kg m^{-3}
μ	Viscosity, kg s^{-1}m^{-1}
μ_0	Magnetic permeability, H m^{-1}
φ	Electric potential, V
η	Overpotential, V
σ	Electrical conductivity, S m^{-1}
σ_{Slag}	Electrical conductivity of slag, S m^{-1}
$\sigma_{Electrode}$	Electrical conductivity of electrode, S m^{-1}
$\sigma_{Crucible}$	Electrical conductivity of crucible, S m^{-1}
σ_{Air}	Electrical conductivity of air, S m^{-1}

REFERENCES

1. B. Hernandez-Morales and A. Mitchell: *Ironmak. Steelmak.*, 1999, vol. 26, pp. 423–38.
2. A. Kharicha, E. Karimi-Sibaki, M. Wu, A. Ludwig, and J. Bohacek: *Steel Res. Int.*, 2018, vol. 89, pp. 1–20.
3. A. Mitchell: *Ironmak. Steelmaak.*, 1974, vol. 3, pp. 172–79.
4. D.A.R. Kay and R.J. Pomfret: *J. Iron Steel Inst.*, 1971, vol. 12, pp. 962–65.
5. K. Fezi, J. Yanke, and M.J.M. Krane: *Metall. Trans. B*, 2015, vol. 46, pp. 766–79.
6. A. Jardy and D. Ablitzer: *Mat. Sci. Tech.*, 2009, vol. 25, pp. 163–69.
7. K.O. Yu, J.A. Domingue, G.E. Maurer, and H.D. Flanders: *JOM*, 1986, vol. 38, pp. 46–50.
8. M.E. Peover: *J. Inst. Metals*, 1972, vol. 100, pp. 97–106.
9. M. Etienne: *The Loss of Reactive Elements During Electroslag Processing of Iron-Based Alloys*, UBC, Canada, 1971.
10. M. Kawakami, K. Nagata, M. Yamamura, N. Sakata, Y. Miyashita, and K.S. Goto: *Testsu-to-Hagane*, 1977, vol. 63, pp. 2162–71.
11. E. Karimi-Sibaki, A. Kharicha, M. Wu, A. Ludwig, and J. Bohacek: *Steel Res. Int.*, 2017, vol. 88, p. 1700011.
12. E. Karimi-Sibaki, A. Kharicha, M. Wu, A. Ludwig, and J. Bohacek: *Ionics*, 2018, vol. 24, pp. 2157–65.
13. A. Mitchell and G. Beynon: *Matall. Trans.*, 1971, vol. 2, pp. 3333–45.
14. G. Beynon: *The Electrochemical Aspects of D.C. Electroslag Remelting*. UBC, Canada, 1967.
15. M. Kato, K. Hasegawa, S. Nomura, and M. Inouye: *Trans. ISIJ*, 1983, vol. 23, pp. 618–27.
16. Y. Kojima, M. Kato, T. Toyoda, and M. Inouye: *Trans. ISIJ*, 1975, vol. 15, pp. 397–406.
17. M.E. Fraser and A. Mitchell: *Ironmak. Steelmak.*, 1976, vol. 5, pp. 279–87.
18. X. Huang, B. Li, and Z. Liu: *Metall. Mater. Trans B*, 2018, vol. 49, pp. 709–22.
19. Q. Wang, G. Li, Z. He, and B. Li: *App. Therm. Eng.*, 2017, vol. 114, pp. 874–86.
20. E.J.F. Dickinson, H. Ekstrom, and E. Fontes: *Electrochem. Commun.*, 2014, vol. 40, pp. 71–74.
21. E. Karimi-Sibaki, A. Kharicha, M. Wu, A. Ludwig, and J. Bohacek: *J. Electrochem. Soc.*, 2018, vol. 165, pp. E604–15.
22. M. Rosales and J.L. Nava: *J. Electrochem. Soc.*, 2017, vol. 164, pp. E3345–53.
23. M. Allibert, H. Gaye, J. Geiseler, D. Janke, B.J. Keene, D. Kirner, M. Kowalski, J. Lehmann, K.C. Mills, D. Neuschütz, R. Parra, C. Saint-Jours, P.J. Spencer, M. Susa, M. Tmar, and E. Woermann: *Slag Atlas*, Verlag Stahleisen GmbH, Düsseldorf, 1995.
24. A. Mitchell and J. Cameron: *Metall. Trans.*, 1971, vol. 2, pp. 3361–66.
25. W. Chiho and X. Shunhua: *ISIJ Int.*, 1993, vol. 33, pp. 239–44.
26. J. Newman and K.E. Thomas-Alyea: *Electrochemical System*, Wiley, New Jersey, 2004.
27. E. Karimi-Sibaki, A. Kharicha, M. Wu, A. Ludwig, and J. Bohacek: *Appl. Math. Comput.*, 2019, vol. 357, pp. 357–73.
28. M. Barati and K.S. Coley: *Metall. Mater. Trans. B*, 2006, vol. 37B, pp. 51–60.
29. H. Song and N. Ida: *IEEE Trans. Magn.*, 1991, vol. 27, pp. 4012–15.
30. E. Karimi-Sibaki, A. Kharicha, J. Bohacek, M. Wu, and A. Ludwig: *Metall. Mater. Trans. B*, 2015, vol. 46B, pp. 2049–61.
31. H. Versteeg and W. Malalasekera: *An Introduction to Computational Fluid Dynamics: The Finite*, Pearson Education Limited, Essex, 2007, vol. Method.
32. B. Van Leer: *J. Comput. Phys.*, 1979, vol. 32, pp. 101–36.
33. T.S. Coffey, C.T. Kelley, and D.E. Keyes: *SIAM J. Sci. Comput.*, 2003, vol. 25, pp. 553–69.
34. G.S. Picard, F.C. Bouyer, M. Leroy, Y. Bertaud, and S. Bouvet: *J. Mol. Struct.*, 1996, vol. 368, pp. 67–80.
35. B. Birol, G. Polat, and M. Saridede: *JOM*, 2015, vol. 67, pp. 427–35.